Journal of Materials Science & Technology 31 (2015) 573–580

Contents lists available at ScienceDirect

Journal of Materials Science & Technology

journal homepage: www.jmst.org

Synthesis, Properties, and Biological Application of Perfect Crystal Gold Nanowires: A Review

Mijeong Kang [1], Hyoban Lee [1], Taejoon Kang [2], Bongsoo Kim [1,*]

[1] Department of Chemistry, KAIST, Daejeon 305-701, Korea
[2] BioNanotechnology Research Center and BioNano Health Guard Research Center, KRIBB, Daejeon 305-806, Korea

ARTICLE INFO

Article history:
Received 25 November 2014
Received in revised form
21 January 2015
Accepted 22 January 2015
Available online 20 March 2015

Key words:
Nanomaterials
Nanostructured metallic materials
Nanowire
Single crystal
Biomedical applications

In the last decade, numerous kinds of nanoscale materials have been created. Their characteristics are critically influenced by their synthetic or fabrication methods. In this review article, we introduce perfect crystal gold nanowires (Au NWs) synthesized by vapor transport method and summarize their material properties and biological applications. Single-crystalline Au NWs having no defects or twins show unique mechanical, electrical, and electrochemical characteristics. Notably, they are exceptionally competent in penetrating cells or tissues with minimum biological damage and in the electrical analysis and manipulation of biological activities in the cells and/or tissues. It is expected that the Au NWs would give us technological breakthrough in diverse applications such as nanoscale functional components as well as new insights in fundamental material science.

1. Introduction

Last few decades have witnessed giant growth in syntheses and applications of nanoscale materials featured by unique and superb material properties compared to their bulk counterparts. Especially, one dimensional (1D) nanomaterials such as nanowire (NW), nanotube, or nanopillar have attracted great attention due to their excellent performances in transporting electronic, optical, and thermal energy and/or signals[1–12], which can be seen from the gradual increase in the number of related publications (Fig. 1). These nanomaterials have nanoscale diameter, which is kept constant along the whole structure. Consequently, they are recently employed to penetrate or interface with living cells or tissues and then to explore and manipulate their biology with high spatial resolution as well as minimum deterioration of their viability[13,14]. For example, semiconducting nanowires have been fabricated into nanoscale transistors and inserted into a living cell to measure its electrical activities[15].

Metallic 1D nanomaterials have great potential in electrical, electrochemical and optical applications[16,17]. Wide-spread research on them, however, has been impeded, to some extent, due to the difficulties in synthesizing and manipulating them. It is surprising that many of them have been fabricated by depositing thin metallic layer onto non-metallic 1D nanomaterials such as boron nitride nanotube due to the lack of facile route to synthesize them[18]. While diverse semiconducting 1D nanomaterials have been grown from metal nanoparticles as catalyst by the well-established vapor-liquid-solid methods[11], there are no reports on the synthesis of metallic ones using such methods since it is hard to find proper catalyst particles for them. Solution phase synthetic methods have successfully produced metallic 1D nanomaterials, which leaves some post-synthetic processes to manipulate them: separating appropriate nanomaterials from their bundle or removing the stabilizing agents attached on their surface.

Among various metallic 1D nanomaterials, gold (Au) NWs offer interesting applications with a number of advantages such as chemical inertness, biocompatibility, and high electrical conductivity. Their utilization has been promoted with the development of various fabrication methods: chemical reduction of Au precursor[19], electrodeposition of Au in confined space[20–22], lithography/lift-off process[23], and slicing thin Au film[24]. Nevertheless, there are some limitations to wide usage of them due to the absence of robust methods for fabricating high-quality Au NWs. The fabrication methods themselves have critical influence on the material properties. In this review, we introduce the defect-free

* Corresponding author. Prof., Ph.D.; Tel.: +82 10 48012836; Fax: +82 42 3502810.
E-mail address: bongsoo@kaist.ac.kr (B. Kim).

http://dx.doi.org/10.1016/j.jmst.2015.01.007

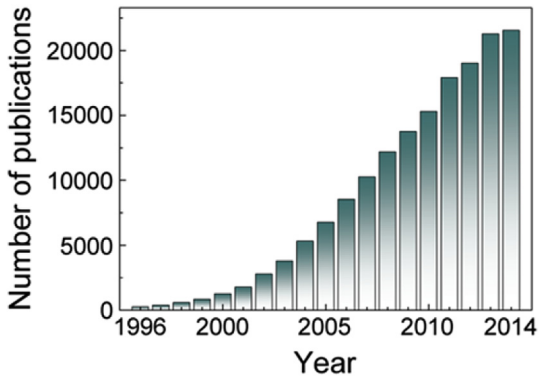

Fig. 1. Number of publications on nanowire, nanotube or nanopillar for 1996–2015 (Source, ISI).

single-crystalline Au NWs synthesized by a vapor transport method. Their unique material characteristics and applications, especially in biological fields are summarized.

2. Synthesis of Single-crystalline Au Nanowires

The Au NWs can be synthesized by a simple vapor transport method[25]. In a horizontal quartz tube furnace, Au atoms are vaporized from the Au slug placed at the middle of a heating zone and transported via carrier gas to sapphire substrates placed a few centimeters downstream (Fig. 2(a)). Au vapors are condensed on the substrates to form nanocrystalline Au seeds and the Au atoms subsequently supplied are deposited on the seeds to grow into nanowires. The direction of NW growth, either vertical (marked by red dotted-contour in Fig. 2(b)) or horizontal to the substrate, can be steered by controlling the atom flux (Fig. 2(b)). The width and length of Au NWs can be controlled by adjusting reaction time. Vertical Au NWs (Fig. 2(c)) are highly useful allowing us to pick up and manipulate a single NW. The synthesized Au NWs are defect-free single-crystalline as confirmed by the electron diffraction pattern (Fig. 2(d)) and are all enclosed by atomically smooth surfaces.

3. Material Characterization of Au Nanowires

3.1. Mechanical characteristics

The intrinsic mechanical properties of materials are related to their atomic movements under mechanical stresses, which is subject to its crystal quality such as density of defects. Defectless single-crystalline Au NWs have unique mechanical characteristics and behavior: superstrong, superplastic and superflexible[26–28]. As a Au NW is pulled and undergoes tensile deformation (Fig. 3(a)), it shows a yield strength of 1.54 GPa (point P1 in a stress–strain curve, Fig. 3(b)), which is significantly higher than that of bulk Au (55–200 MPa) and close to a theoretical limit (1.8 GPa). This superstrength is attributed to the perfectly crystalline nature of Au NWs, making the initial nucleation of dislocations in NWs difficult. Once dislocations are formed in the NWs, they coherently extend to a long distance via twin propagation that converts the <110> NW with a rhombic cross section and {111} side facets to a <100> NW with a rectangular cross section and {100} side facets, resulting in superplastic elongation (Region 2 in Fig. 3(b)). When compressive stress is applied, the Au NW flexibly bends even into a U-shape and completely recovers its

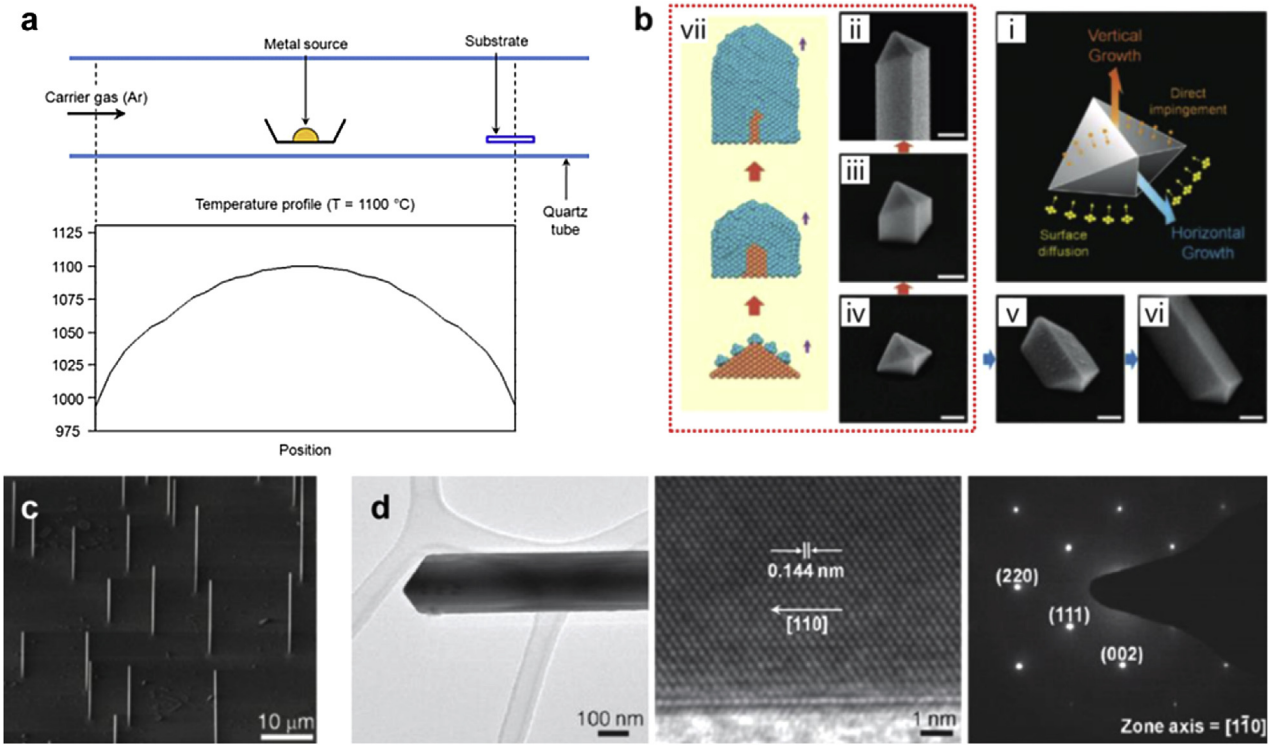

Fig. 2. (a) Schematic representation of the experimental set-up for synthesizing single-crystalline Au NWs. (b) Scanning electron microscope (SEM) and molecular dynamics (MD) images showing the vertical (enclosed by red dotted line) or horizontal growth process of Au NWs. Scale bars in (ii–vi) are 100 nm. (c) 45° tilted SEM image of vertically grown Au NWs. (d) Transmission electron microscope (TEM, left) and high-resolution TEM (middle) images and selected area electron diffraction pattern (right) of a Au NW. Reproduced from ref.[25].

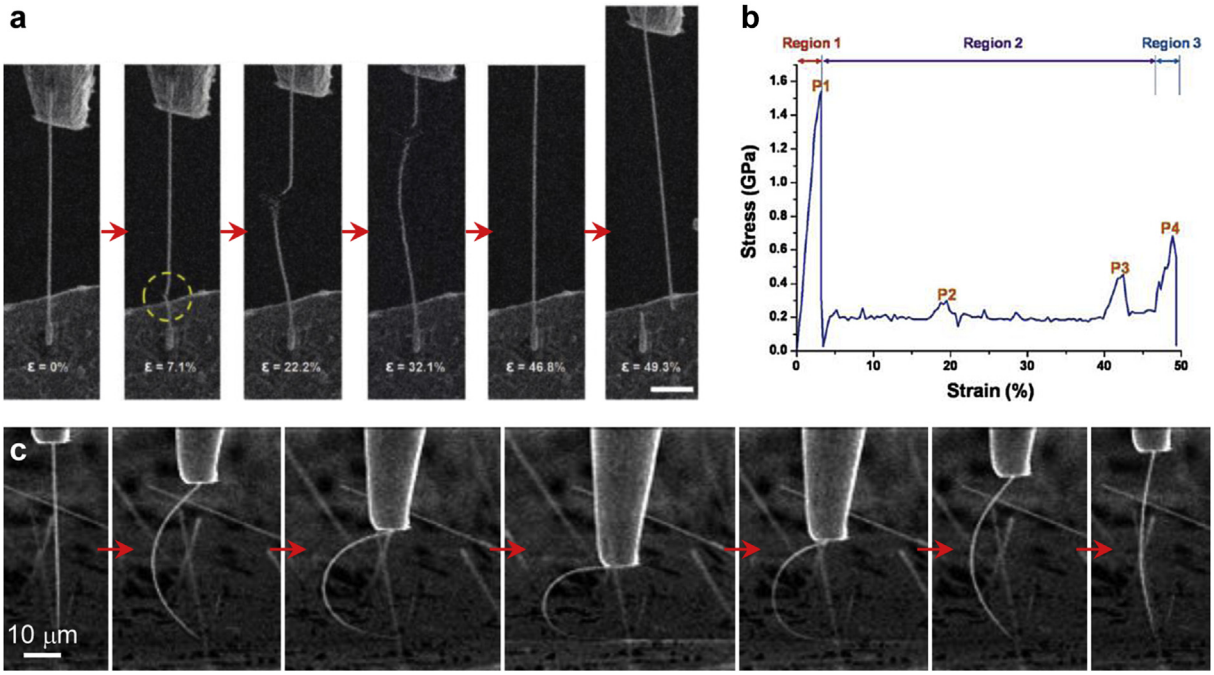

Fig. 3. (a) SEM images taken during the tensile deformation of a Au NW. Reproduced from ref. [26]. Scale bar is 1 μm. (b) Stress-strain curve of a Au NW under tensile stress. Reproduced from ref. [26]. (c) SEM images showing U-shape bending and complete recovery of a Au NW while pushed against and withdrawn from a solid surface. Reproduced from ref.[29].

original shape after the stress is removed as shown in Fig. 3(c) [29]. The combination of these mechanical properties would make the Au NW an interesting functional element in nanomechanical devices.

3.2. Electrical characteristics

A single Au NW shows electrical resistance of 52 Ω as shown in current–voltage (I–V) curve (Fig. 4) obtained from a four-probe device (inset in Fig. 4)[29]. It has electrical resistivity of 2.08×10^{-8} Ωm that is slightly lower than those of bulk Au (2.21×10^{-8} Ωm). It should be noted that this resistivity is also lower than those of other kinds of Au NWs; skived from an insulator-Au thin film-insulator block (~8×10^{-8} Ωm)[24], fabricated by lithography (~6×10^{-8} Ωm)[30] and by electrodeposition (2.26×10^{-8} Ωm)[31]. This lower electrical resistivity of a Au NW is ascribed to its single-crystalline feature without defects or grain boundaries that hinder electron transport.

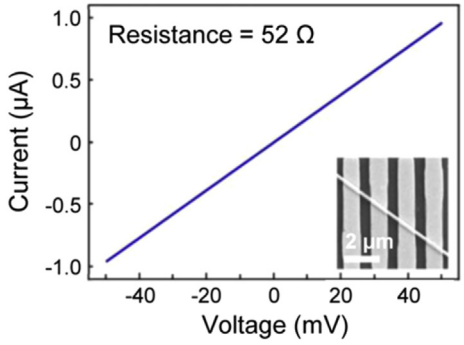

Fig. 4. I–V curve measured from a single Au NW. Inset shows the SEM image of four-probe Au NW device for I–V measurement. Reproduced from ref.[29].

3.3. Electrochemical characteristics

Nanoscale materials have been utilized as nanoelectrodes that can provide important electrochemical applications such as precise electrochemical imaging, highly active catalysis, or single molecule/nanoparticle research which are hardly obtainable from macroscopic electrodes. To use a single Au NW as a nanoelectrode, it is necessary to acquire its fundamental electrochemical characteristics. A Au NW electrode can be fabricated by attaching the single NW to a macroscopic tungsten tip for facile handling (Fig. 5(a))[32]. Then the tungsten tip should be completely insulated to avoid the unwanted reaction or noise from the tungsten surface (Fig. 5(a)). In the cyclic voltammogram (CV) measured in a sulfuric acid solution, sharp single peaks for electrochemical oxidation and reduction of a Au NW are shown at ~0.9 and ~0.4 V, respectively, confirming that the Au NW is enclosed by well-defined single-crystalline surfaces (Fig. 5(b)). The sigmoidal CV measured from a Au NW electrode in a ferricyanide solution indicates that mass transport toward the Au NW occurs fast via convergent diffusion rather than linear one due to its small dimension (Fig. 5(c)). The average impedance of Au NW electrodes measured at 1 kHz in phosphate buffered saline solution is 5.6 MΩ (Fig. 5(d))[29].

4. Biological Application of Au Nanowires

Au NWs have several features, which make them one of the ideal tools for penetrating cell or tissue to analyze and manipulate their biological activities as follows. First, they have a well-defined chisel-like sharp tip that facilitates perforating the cell membrane or going through the tissue by reducing cutting force[33]. Second, their cylindrical geometry with significantly small diameter minimizes the invasiveness of their insertion. Third, they are not only strong enough to penetrate into cells or tissue but also highly flexible to deflect around harder region and pass through softer one, which minimizes deformation of cells or tissue[34,35]. The

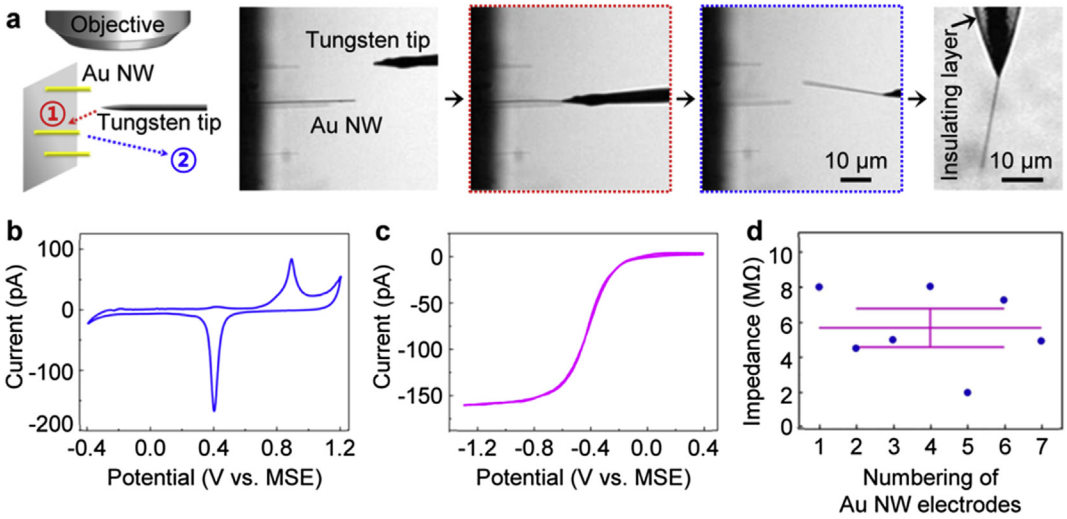

Fig. 5. (a) Schematic representation and optical images showing the process of fabricating a Au NW electrode. (b) CV of a Au NW electrode measured in a 50 mmol/L sulfuric acid solution at a scan rate of 50 mV/s. (c) CV of a Au NW electrode in a 20 mmol/L $K_3Fe(CN)_6$ solution without supporting electrolyte at a scan rate of 200 mV/s. (d) The electrical impedances of Au NW electrodes ($n = 7$) measured at 1 kHz. The error bar (magenta line) represents standard deviation. Reproduced from ref.[32].

Table 1
Characteristics of various nanoinjectors

Nanoinjector material	How to release payload	Site of delivery	Payload material	Ref.
Carbon nanotube	pH-dependent chemical cleavage of disulfide bond	Not controlled	Quantum dot	[38]
BN nanotube	pH-dependent chemical cleavage of disulfide bond	Cytoplasm or nucleus	Quantum dot	[39]
BN nanotube	Electrochemical cleavage of Au–S bond	Cytoplasm or nucleus	Quantum dot	[40]
SnO_2 nanowire	Light-induced cleavage of photocleavable linkage	Cytoplasm or nucleus	Quantum dot	[41]
Si nanowire	Diffusion	Not controlled	Nucleic acids, protein, peptide, small molecule	[42]
Au nanowire	Electrochemical cleavage of Au–S bond, electrophoretic detachment of electrostatically attached payloads	Cytoplasm or nucleus	Nucleic acids	[32]

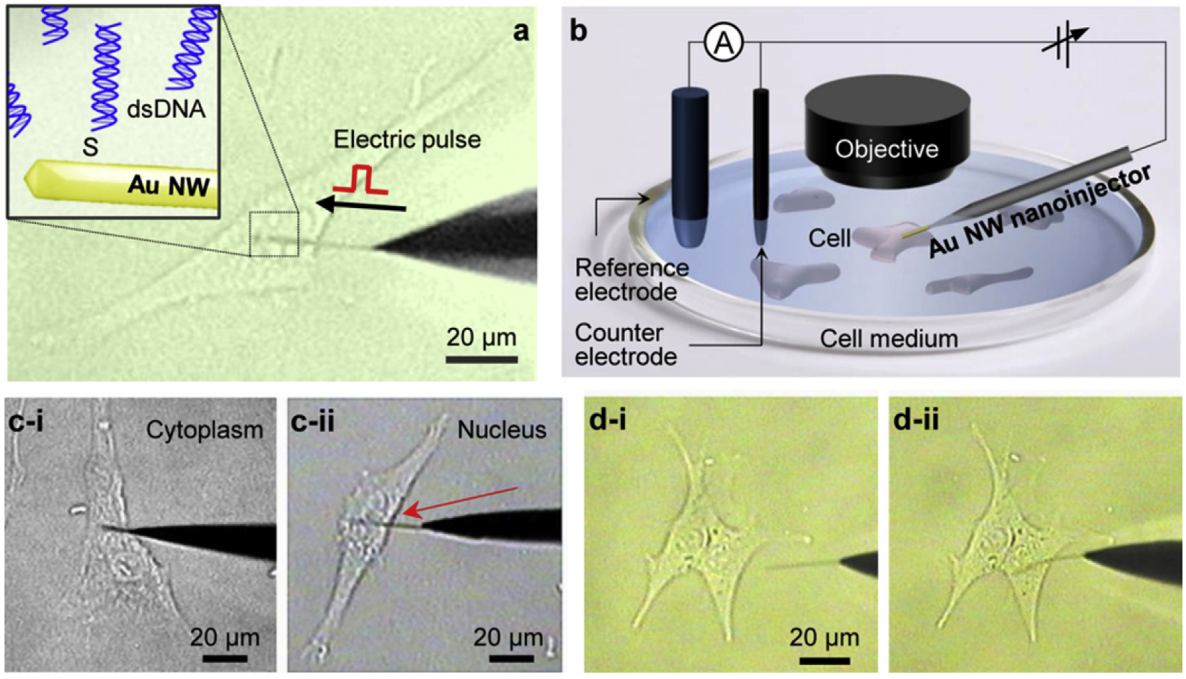

Fig. 6. (a) Schematic representation of electrically triggered gene delivery into the nucleus of a living cell using a Au NW nanoinjector. (b) Schematic representation of the experimental set-up for Au NW nanoinjector-based intracellular delivery system. (c) Optical images showing the insertion of a Au NW nanoinjector into cytoplasm (c-i) and nucleus (c-ii). (d) Optical images showing the flexible insertion of a Au NW nanoinjector (from d-i to d-ii). Reproduced from ref.[32].

combination of these unique properties makes the insertion of Au NWs into biological components highly biocompatible.

4.1. Nanoinjector for intracellular delivery

Delivering exogenous materials into a cell is of great importance in fundamental cell biology and advanced applications such as drug development or cell engineering. Among diverse types of delivery methods, direct intracellular injection of exogenous materials is superior in terms of delivery efficiency and universal applicability regardless of cell type[36]. One of the most important features required for intracellular injectors, which are inserted inside the cell, is their small dimension so as to minimize damage to the living cells. In addition, as their dimension is reduced, the spatial resolution of delivery is increased, which could be beneficial to the function of delivered materials by properly releasing them at the site of action[37]. In this sense, there have been developed diverse nanoscale intracellular injectors (nanoinjectors) using 1D nanomaterials as listed in Table 1[32,38–42]. They can maintain cellular integrity during and after the delivery.

Material characteristics of the nanoinjectors have influence on the important processes in delivery such as loading and releasing exogenous materials and getting access to specific intracellular region. A Au NW nanoinjector can deliver various exogenous materials attached on the NW via Au–S covalent bond to the specific site of a living cell by electrical triggering that electrochemically cleaves the Au–S bond[32]. For example, DNA can be delivered into a cell nucleus as illustrated in Fig. 6(a). The delivery system is composed of a Au NW nanoinjector (working electrode), a saturated calomel electrode (reference electrode), and a Pt wire (counter electrode) for three-electrode configuration; of a nanomanipulator for controlling the position of the nanoinjector; and of an optical microscope for monitoring whole delivery process (Fig. 6(b)). The Au NW nanoinjector can be precisely inserted into a specific intracellular position, for example, either cytoplasm (Fig. 6(c-i)) or nucleus (Fig. 6(c-ii)). This insertion is mechanically compliant with cells as shown in Fig. 6(d), where the Au NW flexibly bends upon entering the cell to deflect around relatively rigid intracellular structures, which minimizes cellular deformation.

For efficient and biocompatible DNA delivery via electrical triggering, voltage and duration of electrical pulse were optimized as follows. Thiolated DNA with fluorescent dye intercalated was attached on the Au NW nanoinjectors via Au–S bond (Fig. 7(a)) and an electric pulse with different voltage and duration was applied to each of the nanoinjector to reductively cleave the Au–S bond. The extent of DNA detachment was examined by observing fluorescence from remaining dye-intercalated DNA on the nanoinjector (Fig. 7(b)). The most benign electrical pulse that induces almost complete detachment of DNA was found to be −0.8 V pulse applied for 2 min (Fig. 7(c)).

Successful intracellular DNA delivery and the expression of the delivered DNA can be verified with green fluorescent protein (GFP)-coding DNA. The thiolated linear DNA that coded for GFP was directly attached on Au NW nanoinjectors via Au–S bond and the plasmid that coded for GFP was attached via electrostatic attraction after modifying the surface of the Au NW with thiolated cationic molecules. Each of these nanoinjectors was inserted into a cell nucleus and then the optimized electric pulse was applied to the nanoinjectors. In both cases, green fluorescence was observed from the cell where GFP-coding DNA was injected, indicating successful expression of the delivered DNA (Fig. 8). This implies that Au NW nanoinjectors can deliver various exogenous materials due to their abilities in diverse surface modification without deteriorating cellular function.

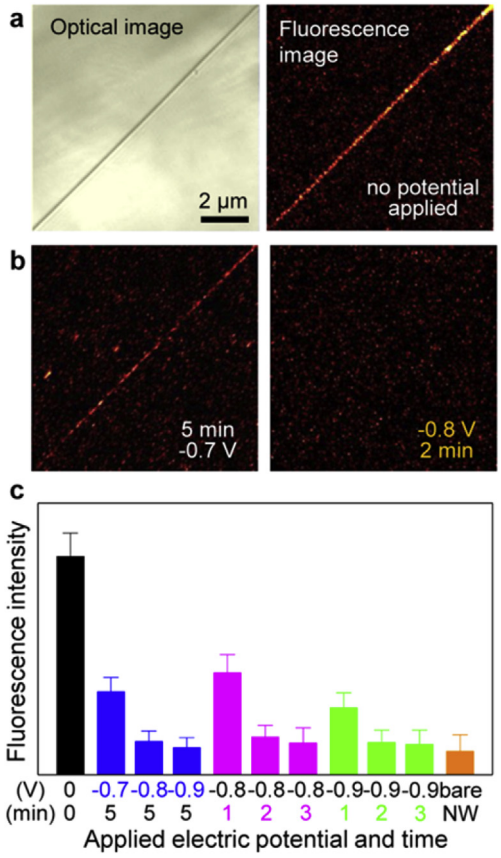

Fig. 7. (a) Optical (left) and fluorescence (right) images of the Au NW on which fluorescent dye-intercalated DNA is attached. (b) Fluorescence images of Au NWs where fluorescent dye-labeled DNA is firstly attached and then detached by electric pulses of different potential and duration as written in the images. (c) Fluorescence intensities remaining on the Au NW nanoinjectors after detaching fluorescent dye-intercalated DNA by electric pulses of different potential and duration. Reproduced from ref.[32].

This Au NW nanoinjector-based delivery system does not limit the types of cells and delivered exogenous materials. It is expected that the Au NW nanoinjector would be widely used in various applications such as the development of therapeutic agents that act

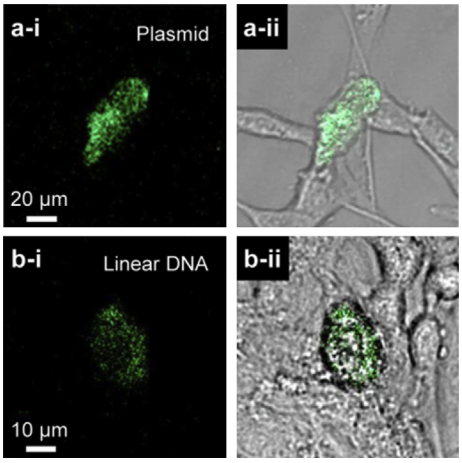

Fig. 8. (a) Fluorescence (a-i) and merged fluorescence/optical (a-ii) images of the cell into which GFP-coding plasmid was delivered. (b) Fluorescence (b-i) and merged fluorescence/optical (b-ii) images of the cell into which GFP-coding linear DNA was delivered. Reproduced from ref.[32].

inside cells as well as the fundamental biological studies on cellular response to the specific exogenous materials.

4.2. Nanoprobe for neural recording

Understanding neural activity is essential to treat many diseases caused by degeneration and malfunction occurring in nervous system. To record neural signal, electrodes implanted in brain have been developed with various materials such as metal, silicon, and metal oxide[43–50]. Although there have been continuous efforts to increase the spatial resolution of neural recording by reducing the size of the conventional electrodes, it is difficult to avoid the deterioration of their mechanical strength and electrical conductivity, which are important for implanting the electrode and collecting neural signal, respectively. Recently, nanomaterials such as carbon nanotubes, silicon nanowires, or gold nanoparticles were employed to fabricate neural electrodes, allowing the successful miniaturization of the electrode without sacrificing material properties[15,51–61]. Single-crystalline Au NWs possessing superflexibility as well as superstrength, high electrical conductivity, and well-defined geometry with sharp tip can potentially be ideal neural electrode materials.

Neural signals in the brain of a freely moving mouse were measured from two Au NW electrodes (diameter: 100 nm, length: 5 μm) implanted separately within 1 mm (Fig. 9(a)). Representative neural signals distinctly show characteristic neural spikes (Fig. 9(b-i)). It should be noted that the two signals are clearly different, implying that Au NW electrodes can distinguish neural signals of 1 mm-separated regions. Their interdependence can be quantified by cross-correlation analysis, which gives higher correlation coefficient as the similarity of two signals increases (Fig. 9(b-ii)). In comparison, two tungsten electrodes having a tapered shape (diameter in the middle part: 1 μm, length: 5 μm) were implanted as the same as Au NW ones. They recorded similar baseline oscillation as Au NW electrodes but hardly captured neural spikes (Fig. 9(c-i)). Signals measured from two tungsten electrodes are quite similar as indicated by cross-correlation analysis (Fig. 9(c-ii)). Significant difference in the averaged first-peak values of

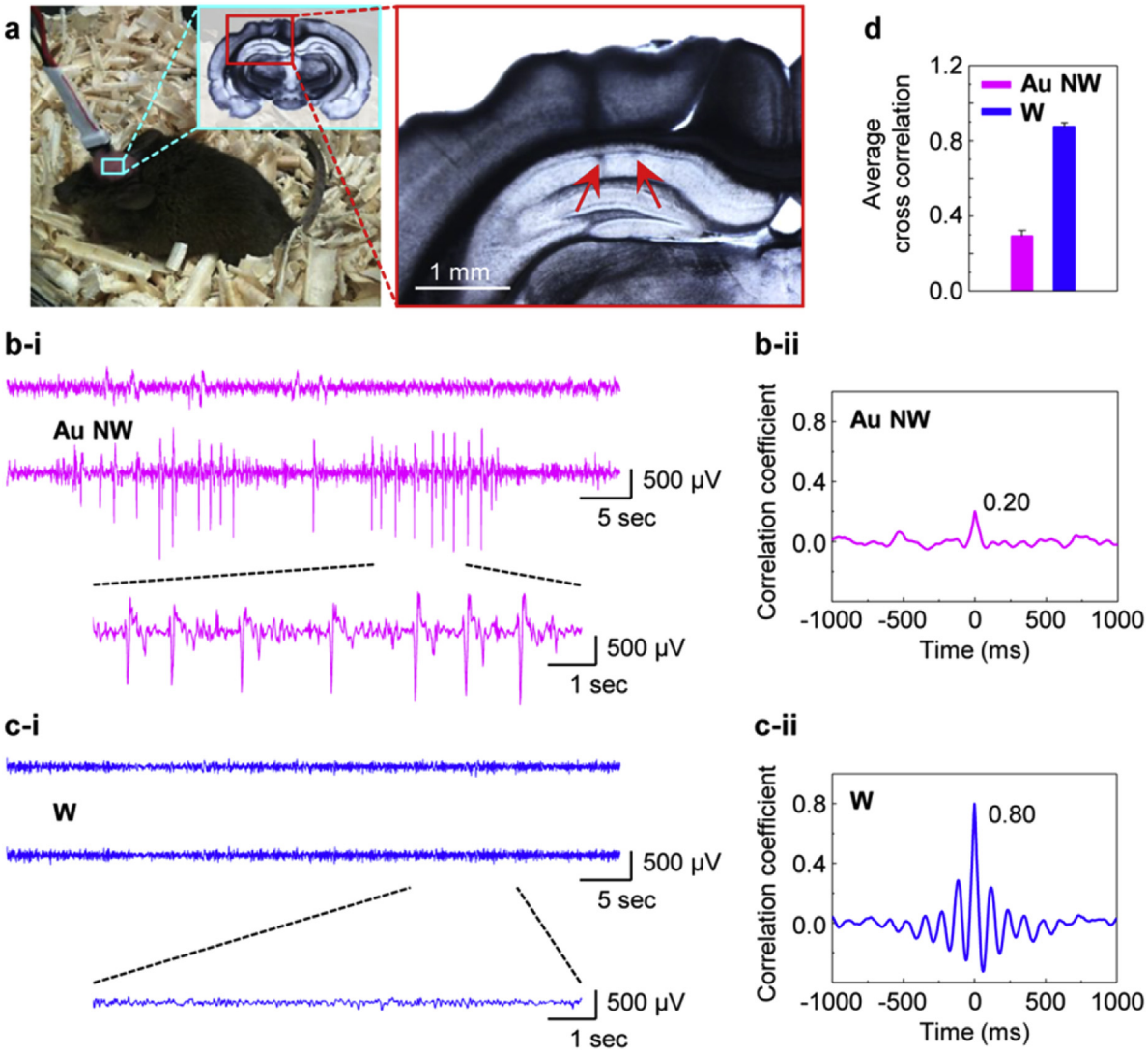

Fig. 9. (a) Photograph of a mouse with Au NW electrodes implanted in its brain (left). Post-mortem histology of the recording regions and a brain slice showing the positions (arrows) of the electrodes (right). (b) Representative traces of neural signals recorded by two Au NW electrodes implanted within 1 mm apart (b-i) and the corresponding cross-correlation analysis (b-ii, first-peak value: 0.20). (c) Representative traces of neural signals recorded by two tungsten electrodes implanted within 1 mm apart (c–i) and the corresponding cross-correlation analysis (c-ii, first-peak value: 0.80). (d) Average first-peak values of the correlation coefficient for Au NW ($n = 6$) and tungsten ($n = 8$) electrodes. Reproduced from ref.[29].

correlation coefficient means that Au NW electrodes could provide much higher spatial resolution than tungsten electrodes.

One of the most interesting features of Au NW electrodes is that they can record high-quality neural signals from ~1 h after the implantation while general neural electrodes require a few days to begin recording[62]. This could be attributed to the reduced neural damage around the Au NW owing to their small dimension and mechanical compliance with soft brain tissues, which would dramatically shorten the post-implantation recovery period.

The high-quality neural recording from Au NW electrodes facilitate the extraction of more biological information from the signals as following two exemplary demonstrations. First, a mouse with recording electrodes, either Au NW electrodes or tungsten ones, was confronted with an unfamiliar mouse in its confined territory and the neural signals before (Fig. 10(a)) and after (Fig. 10(b)) the encounter were compared. Au NW electrodes captured the increase in neural spikes after the encounter, which indicates the excited status of the mouse. With the tungsten electrodes, it was difficult to sense discernible changes in neural signals.

Second, the spatial resolution of localizing the seizure focus using Au NW and tungsten electrodes was compared. The mouse with three Au NW electrodes implanted separately by 1 mm was given pilocarpine, which induces epilepsy. Epilepsy is one of the most common neurological diseases and characterized by seizure episodes generated from a specific seizure focus. Three Au NW electrodes recorded different neural activities and one of them captured distinct spike activities (middle trace in Fig. 10(c)). The same experiment was conducted with three tungsten electrodes and it is difficult to find difference in the signals from them (Fig. 10(d)). These results indicated that Au NW electrodes distinguish three separated local region and, therefore, could locate seizure focus with much enhanced spatial resolution than microscopic tungsten electrodes.

The significantly small size of Au NW electrodes would open the doorway for much better understanding of brain functions and consequently, for the improvement of the treatment strategies for nervous diseases. It is also anticipated that the Au NW electrodes could be employed for diverse bio/medical/chemical studies including neural signal recordings, neural stimulation, and in vivo monitoring of brain chemistry and electrochemistry.

5. Conclusions and Perspectives

In this review, we introduced the Au NWs synthesized by vapor transport method and summarized their unique material characteristics originating from the defectless single-crystalline nature and their applications on cell and tissue biology. Perfect cylindrical structure with highly small diameter and mechanically strong as well as flexible nature of Au NWs allow them to penetrate cells and tissue with minimum invasiveness and their high electrical conductivity facilitates the transmission of electrical energy and the detection of electrical signal. By virtue of these features, Au NWs can deliver exogenous materials into specific subcellular organelles of a cell upon electrical triggering and record electrical neural signal in the animal brain with high sensitivity and spatial resolution.

The Au NWs can play key functional roles in other interesting applications regarding the analysis and control of various biological phenomena. For example, it is possible to harvest solar energy from plant cells by inserting the NW electrodes into the cells and directly extracting the electron produced during their photosynthesis[63]. Au NWs could be excellent extractors due to their biocompatibility and minimum invasiveness. Au NW electrodes can detect redox-active biomolecules inside and outside cells. They can monitor exocytosis of redox-active signaling molecules released from a secretory cell with significantly high spatial resolution[64]. Surface modification of Au NWs would enlarge the

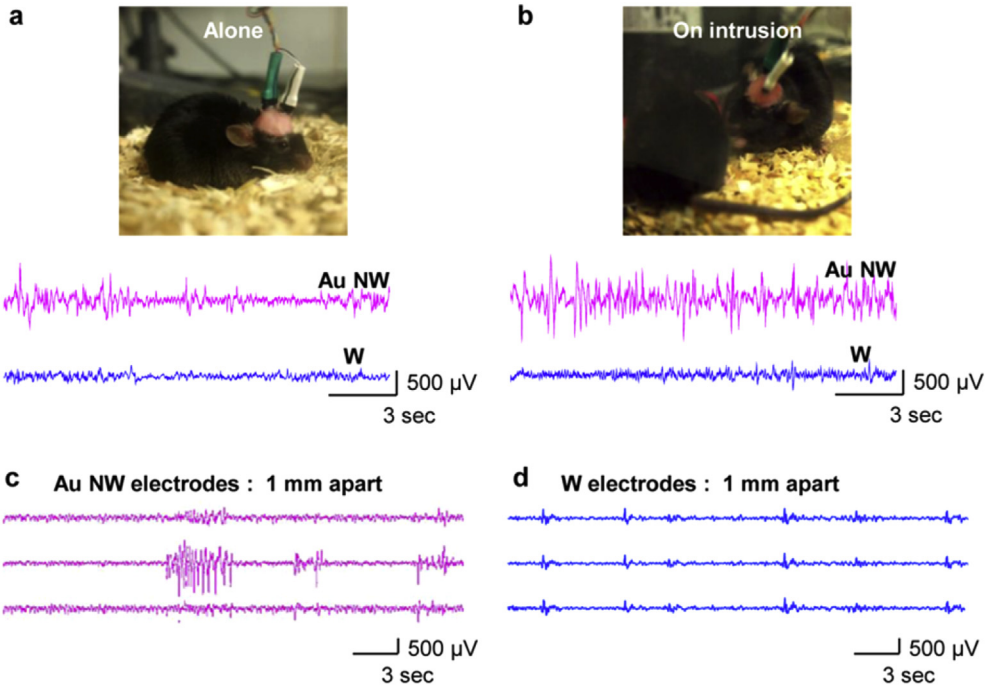

Fig. 10. (a) Representative traces of neural signals recorded from Au NW (upper) and tungsten (lower) electrodes implanted in the mouse moving alone as shown in the photograph. (b) Representative traces of neural signals recorded from Au NW (upper) and tungsten (lower) electrodes implanted in the mouse faced with an unfamiliar mouse as shown in the photograph. (c) Pilocarpine-induced seizure signals recorded by three Au NW electrodes separately implanted by 1 mm in the mouse brain. (d) Pilocarpine-induced seizure signals recorded by three tungsten electrodes separately implanted by 1 mm in the mouse brain. Reproduced from ref.[29].

realm of their applications. Redox-inactive biomolecules also can be detected by the Au NW electrode, of which surface is modified with the capture agent that recognizes target biomolecules and with the signaling agent that transduces the capture event into the electrochemical signal[65]. Insulating the side wall of a Au NW could result in the nanoscale patch clamp that enables cytocompatible physiological studies[66]. Such nanoscale patch clamp can give us long-term monitoring of cell physiology unlike microscale couterparts that easily harm the cellular integrity within half an hour. It is anticipated that Au NWs would significantly contribute to revealing the mechanisms of various biological phenomena and developing the tools and technologies for cellular/tissue engineering.

Acknowledgements

This work was supported by the Public welfare & Safety research program (NRF-2012M3A2A1051686) through the National Research Foundation of Korea funded by the Ministry of Science, ICT & Future Planning (MSIP), Global Frontier Project (H-GUARD_2014M3A6B2060489) through the Center for BioNano Health-Guard funded by the MSIP, and KRIBB initiative Research Program.

References

[1] Y. Xia, P. Yang, Y. Sun, Y. Wu, B. Mayers, B. Gates, Y. Yin, F. Kim, H. Yan, Adv. Mater. 15 (2003) 353–389.
[2] B. Wu, A. Heidelberg, J.J. Boland, Nat. Mater. 4 (2005) 525–529.
[3] B.K. Teo, X.H. Sun, Chem. Rev. 107 (2007) 1454–1532.
[4] Y. Liu, J. Wang, C. Xu, Z. Si, S. Xu, S. Shi, J. Mater. Sci. Technol. 30 (2014) 860–866.
[5] H. Liu, Z. Zhang, L. Hu, N. Gao, L. Sang, M. Liao, R. Ma, F. Xu, X. Fang, Adv. Opt. Mater. 2 (2014) 771–778.
[6] X. Fang, L. Hu, K. Huo, B. Gao, L. Zhao, M. Liao, P.K. Chu, Y. Bando, D. Golberg, Adv. Funct. Mater. 21 (2011) 3907–3915.
[7] Y. Yue, M. Chen, Y. Ju, S. Wang, J. Mater. Sci. Technol. 29 (2013) 1156–1160.
[8] T.Y. Olson, J.Z. Zhang, J. Mater. Sci. Technol. 24 (2008) 433–446.
[9] S. Han, L. Hu, N. Gao, A.A. Al-Ghamdi, X. Fang, Adv. Funct. Mater. 24 (2014) 3725–3733.
[10] L. Sun, D. Zhao, M. Ding, H. Zhao, Z. Zhang, B. Li, D. Shen, J. Mater. Sci. Technol. 29 (2013) 613–618.
[11] P. Yang, R. Yan, M. Fardy, Nano Lett. 10 (2010) 1529–1536.
[12] D. Golberg, Y. Bando, Y. Huang, T. Terao, M. Mitome, C. Tang, C. Zhi, ACS Nano 4 (2010) 2979–2993.
[13] K. Yum, M.F. Yu, N. Wang, Y.K. Xiang, Biochim. Biophys. Acta-Gen. Subj. 1810 (2011) 330–338.
[14] B. Tian, C.M. Lieber, Annu. Rev. Anal. Chem. 6 (2013) 31–51.
[15] B.Z. Tian, T. Cohen-Karni, Q. Qing, X.J. Duan, P. Xie, C.M. Lieber, Science 329 (2010) 830–834.
[16] C.J. Murphy, T.K. Sau, A.M. Gole, C.J. Orendorff, J.X. Gao, L. Gou, S.E. Hunyadi, T. Li, J. Phys. Chem. B 109 (2005) 13857–13870.
[17] J. Chen, X. Wang, Opt. Lett. 39 (2014) 4088–4091.
[18] K. Yum, H. Cho, J. Hu, M.F. Yu, ACS Nano 1 (2007) 440–448.
[19] F. Kim, K. Sohn, J. Wu, J. Huang, J. Am. Chem. Soc. 130 (2008) 14442–14443.
[20] L. Liu, W. Lee, Z. Huang, R. Scholz, U. Gösele, Nanotechnology 19 (2008) 335604.
[21] M. Yun, N.V. Myung, R.P. Vasquez, C. Lee, E. Menke, R.M. Penner, Nano Lett. 4 (2004) 419–422.
[22] E.J. Menke, M.A. Thompson, C. Xiang, L.C. Yang, R.M. Penner, Nat. Mater. 5 (2006) 914–919.
[23] S. Keebaugh, A.K. Kalkan, W.J. Nam, S.J. Fonash, Electrochem. Solid-State Lett. 9 (2006) H88.
[24] K. Dawson, J. Strutwolf, K.P. Rodgers, G. Herzog, D.W.M. Arrigan, A.J. Quinn, A. O'Riordan, Anal. Chem. 83 (2011) 5535–5540.
[25] Y. Yoo, K. Seo, S. Han, K.S.K. Varadwaj, H.Y. Kim, J.H. Ryu, H.M. Lee, J.P. Ahn, H. Ihee, B. Kim, Nano Lett. 10 (2010) 432–438.
[26] J.H. Seo, Y. Yoo, N.Y. Park, S.W. Yoon, H. Lee, S. Han, S.W. Lee, T.Y. Seong, S.C. Lee, K.B. Lee, P.R. Cha, H.S. Park, B. Kim, J.P. Ahn, Nano Lett. 11 (2011) 3499–3502.
[27] J.H. Seo, H.S. Park, Y. Yoo, T.Y. Seong, J. Li, J.P. Ahn, B. Kim, I.S. Choi, Nano Lett. 13 (2013) 5112–5116.
[28] S. Lee, J. Im, Y. Yoo, E. Bitzek, D. Kiener, G. Richter, B. Kim, S.H. Oh, Nat. Commun. 5 (2014) 3033.
[29] M. Kang, S. Jung, H. Zhang, T. Kang, H. Kang, Y. Yoo, J.P. Hong, J.P. Ahn, J. Kwak, D. Jeon, N.A. Kotov, B. Kim, ACS Nano 8 (2014) 8182–8189.
[30] Z. Zou, J. Kai, C.H. Ahn, J. Micromech. Microeng. 19 (2009) 055002.
[31] Y. Peng, T. Cullis, B. Inkson, Appl. Phys. Lett. 93 (2008) 183112.
[32] S.M. Yoo, M. Kang, T. Kang, D.M. Kim, S.Y. Lee, B. Kim, Nano Lett. 13 (2013) 2431–2435.
[33] D.J. Edell, V.V. Toi, V.M. Mcneil, L.D. Clark, IEEE Trans. Biomed. Eng. 39 (1992) 635–643.
[34] S.P. DiMaio, S.E. Salcudean, IEEE Trans. Biomed. Eng. 52 (2005) 1167–1179.
[35] R. Singhal, Z. Orynbayeva, R.V.K. Sundaram, J.J. Niu, S. Bhattacharyya, E.A. Vitol, M.G. Schrlau, E.S. Papazoglou, G. Friedman, Y. Gogotsi, Nat. Nanotechnol. 6 (2011) 57–64.
[36] D.J. Stephens, R. Pepperkok, Proc. Natl. Acad. Sci. USA 98 (2001) 4295–4298.
[37] X.T. Zheng, P. Chen, C.M. Li, Small 10 (2012) 2670–2674.
[38] X. Chen, A. Kis, A. Zettl, C.R. Bertozzi, Proc. Natl. Acad. Sci. USA 104 (2007) 8218–8222.
[39] K. Yum, S. Na, Y. Xiang, N. Wang, M.F. Yu, Nano Lett. 9 (2009) 2193–2198.
[40] K. Yum, N. Wang, M.F. Yu, Small 6 (2010) 2109–2113.
[41] R. Yan, J.H. Park, Y. Choi, C.J. Heo, S.M. Yang, L.P. Lee, P. Yang, Nat. Nanotechnol. 7 (2012) 191–196.
[42] A.K. Shalek, J.T. Robinson, E.S. Karp, J.S. Lee, D.R. Ahn, M.H. Yoon, A. Suttona, M. Jorgollic, R.S. Gertnera, T.S. Gujrala, G. MacBeatha, E.G. Yang, H. Park, Proc. Natl. Acad. Sci. USA 107 (2010) 1870–1875.
[43] K.A. Moxon, S.C. Leiser, G.A. Gerhardt, K.A. Barbee, J.K. Chapin, IEEE Trans. Biomed. Eng. 51 (2004) 647–656.
[44] P.M. Talauliker, D.A. Price, J.J. Burmeister, S. Nagari, J.E. Quintero, F. Pomerleau, P. Huettl, J.T. Hastings, G.A.J. Gerhardt, Neurosci. Meth. 198 (2011) 222–229.
[45] P.K. Campbell, K.E. Jones, R.J. Huber, K.W. Horch, R.A. Normann, IEEE Trans. Biomed. Eng. 38 (1991) 758–768.
[46] A. Peyrache, N. Dehghani, E.N. Eskandar, J.R. Madsen, W.S. Anderson, J.A. Donoghue, L.R. Hochberg, E. Halgren, S.S. Cash, A. Destexhe, Proc. Natl. Acad. Sci. USA 109 (2012) 1731–1736.
[47] J.K. Chapin, K.A. Moxon, R.S. Markowitz, M.A.L. Nicolelis, Nat. Neurosci. 2 (1999) 664–670.
[48] M.A. Wilson, B.L. McNnaughton, Science 261 (1993) 1055–1058.
[49] T.G.H. Yuen, W.F. Agnew, Biomaterials 16 (1995) 951–956.
[50] M.A.L. Nicolelis, D. Dimitrov, J.M. Carmena, R. Crist, G. Lehew, J.D. Kralik, S.P. Wise, Proc. Natl. Acad. Sci. USA 100 (2003) 11041–11046.
[51] H. Zhang, J. Shih, J. Zhu, N.A. Kotov, Nano Lett. 12 (2012) 3391–3398.
[52] Z. Jiang, Q. Qing, P. Xie, R.X. Gao, C.M. Lieber, Nano Lett. 12 (2012) 1711–1716.
[53] X.J. Duan, R.X. Gao, P. Xie, T. Cohen-Karni, Q. Qing, H.S. Choe, B.Z. Tian, X.C. Jiang, C.M. Lieber, Nat. Nanotechnol. 7 (2012) 174–179.
[54] T. Cohen-Karni, D. Casanova, J.F. Cahoon, Q. Qing, D.C. Bell, C.M. Lieber, Nano Lett. 12 (2012) 2639–2644.
[55] E.W. Keefer, B.R. Botterman, M.I. Romero, A.F. Rossi, G.W. Gross, Nat. Nanotechnol. 3 (2008) 434–439.
[56] G. Cellot, E. Cilia, S. Cipollone, V. Rancic, A. Sucapane, S. Giordani, L. Gambazzi, H. Markram, M. Grandolfo, D. Scaini, F. Gelain, L. Casalis, M. Prato, M. Giugliano, L. Ballerini, Nat. Nanotechnol. 4 (2009) 126–133.
[57] J.T. Robinson, M. Jorgolli, A.K. Shalek, M.H. Yoon, R.S. Gertner, H. Park, Nat. Nanotechnol. 7 (2012) 180–184.
[58] T. Cohen-Karni, Q. Qing, Q. Li, Y. Fang, C.M. Lieber, Nano Lett. 10 (2010) 1098–1102.
[59] R.X. Gao, S. Strehle, B.Z. Tian, T. Cohen-Karni, P. Xie, X.J. Duan, Q. Qing, C.M. Lieber, Nano Lett. 12 (2012) 3329–3333.
[60] K. Fuchsberger, A. Le Goff, L. Gambazzi, F.M. Toma, A. Goldoni, M. Giugliano, M. Stelzle, M. Prato, Small 7 (2011) 524–530.
[61] E. Jan, J.L. Hendricks, V. Husaini, S.M. Richardson-Burns, A. Sereno, D.C. Martin, N.A. Kotov, Nano Lett. 9 (2009) 4012–4018.
[62] X. Tang, L. Yang, L.D. Sanford, Sleep 30 (2007) 1057–1061.
[63] W.H. Ryu, S.J. Bai, J.S. Park, Z. Huang, J. Moseley, T. Fabian, R.J. Fasching, A.R. Grossman, F.B. Prinz, Nano Lett. 10 (2010) 1137–1143.
[64] W. Wang, S.H. Zhang, L.M. Li, Z.L. Wang, J.K. Cheng, W.H. Huang, Anal. Bioanal. Chem. 394 (2009) 17–32.
[65] J. Das, K.B. Cederquist, A.A. Zaragoza, P.E. Lee, E.H. Sargent, S.O. Kelley, Nat. Chem. 4 (2012) 642–648.
[66] M.G. Schrlau, N.J. Dun, H.H. Bau, ACS Nano 3 (2009) 563–568.